New Folder Name LIGO Conceptual Design Handbook 3 Document

DRAFT

FOR INTERNAL USE ONLY

LIGO Interferometer Conceptual Design Handbook

Version 2.0

Authors: LIGO Science Team

October 23, 1992

LIGO-T920001-02-D

Contents

Chapter 1 Introduction 1

1.1 Dimensions and Properties of Initial LIGO Interferometers . 1

1.2 Performance Requirements 1

Shot Noise 4

Seismic Noise 8

Thermal Noise 12

Other Noise Sources 17

1.3 Design Overview 18

Handbook Organization 19

Chapter 2 ICD 2000 Prestabilized Laser 21

2.1 Functional Requirements 21

2.2 Block Diagram and Subsystem Description 23

ICD 2100 Laser 24

ICD 2200 Power Stabilization 24

ICD 2300 Frequency Stabilization 25

2.3 Methods for Testing Subsystem Blocks 26

Test Procedure for ICD 2100 Laser 26

Test Procedure for ICD 2200 Power Stabilization 27

Test Procedure for ICD 2300 Frequency Stabilization . . . 27

2.4 Interfaces 28

Interfaces with Other Subsystems 28

Interfaces with the Environment 28

2.5 Data and Control Signal Definition 29

2.6 Developmental Status 30

Chapter 3 ICD 3000 Mode Cleaner 32
3.1 Functional Requirements 32
3.2 Block Diagram and Subsystem Description 32
ICD 3100 Mode Cleaner Conditioning Optics 32
ICD 3200 Mode Cleaner Modulation 33
ICD 3300 Mode Cleaner Cavity 33
ICD 3400 Mode Cleaner Suspension and Control 33
ICD 3500 Mode Cleaner Seismic Isolation 33
3.3 Methods for Testing Subsystem Blocks 33
3.4 Interfaces 33
3.5 Data and Control Signal Definition 33
3.6 Developmental Status 33

Chapter 4 ICD 4000 Interferometer Conditioning Optics 34
4.1 Functional Requirements 34
4.2 Block Diagram and Subsystem Definition 34
ICD 4100 Conditioning Optics 35
ICD 4200 Conditioning Optics Suspension and Control . . 35
ICD 4300 Conditioning Optics Seismic Isolation 35
4.3 Methods for Testing Subsystem Blocks 35
4.4 Interfaces 35
4.5 Data and Control Signal Definition 35
4.6 Developmental Status 35

Chapter 5 ICD 5000 Optical Interferometer 36

Chapter 6 ICD 6000 Auto Alignment 37

Chapter 7 ICD 7000 Suspension and Control 38

Chapter 8 ICD 8000 Seismic Isolation 39
8.1 Functional Requirements 40
8.2 Subsystem Description and Block Diagram 40
ICD 8100 Test Mass Chamber 1 Seismic Isolation 41

ICD 8200 Test Mass Chamber 2 Seismic Isolation 44
ICD 8300 Diagonal Chamber Seismic Isolation 45
ICD 8400 HAM Seismic Isolation 46
8.3 Method for Testing Subsystem blocks 49
Qualification Testing 49
Acceptance Testing 49
8.4 Interfaces 50
Requirements Placed on Interfaces by Seismic Isolation . . 50
8.5 Developmental Status 50

Chapter 9 Data Acquisition and Interferometer Operations 52

Chapter 10 Environmental Monitoring System 53

Appendix A Scaling of Coalescing Compact Binary Detection Rates with Initial Reciever Noise Parameters 54
A.1 SNR and Detectable Event Rate 54
A.2 Receiver Noise Model 55
Seismic Noise 56
Thermal Noise 56
Shot Noise 56
A.3 Event Spectrum and Detection Rate 57

Bibliography 61

Chapter 1
Introduction

The ICD Handbook lays out the conceptual design for initial LIGO interferometers, as determined by scientific requirements and technical goals. The design is described in terms of subsystems; associated with each subsystem is a set of requirements, specifications, interfaces and tests for qualification. The following topics are not included here: operations scenario, data analysis, subsequent interferometers, work breakdown, schedules, and cost.

The handbook is intended as a reference document for all scientists and engineers working on LIGO.

1.1 Dimensions and Properties of Initial LIGO Interferometers

The key dimensions and physical properties of the initial LIGO interferometers are listed in Table 1.1. The details of the vacuum systems are covered in the 89 Proposal [1]; we list here the dimensions most closely connected to the interferometers.

1.2 Performance Requirements

The initial LIGO interferometers should be sensitive in the frequency band from approximately 30 Hz to approximately 10 kHz. Sensitivity is specified by equivalent displacement noise of interferometer test masses as a function of frequency (displacement amplitude spectral density $\tilde{x}$, units of $\mathrm{m}/\sqrt{\mathrm{Hz}}$), or by strain noise, which is defined as displacement noise divided by interferometer arm length: $\tilde{h}(f) = \tilde{x}(f)/L$. Figure 1.1 shows the expected sensitivity of initial interferometers, and the dominant noise contributors: seismic noise, suspension thermal noise, and shot noise at low, intermediate, and high frequencies, respectively. For comparison with a gravitational signal, it also shows the "most

INTERFEROMETER PHYSICAL PROPERTIES		
PARAMETER	**VALUE**	**NOTES**
Site 1 Arm Length	L =2 km (half-length) L =4 km (full-length)	Multiple interferometers in common vacuum pipe
Site 2 Arm Length	L =4 km	Full-length only
Test Mass Mirrors		
Material	Fused Silica	Test Mass/Mirrors are monolithic. Precise dimensions TBD.
Diameter	≈25 cm	
Thickness	≈10 cm	
Curvatures		
Input Mirrors	Flat	
End Mirrors	R_c = 6 km (full-length) R_c = 3 km (half-length)	
Laser Wavelength	λ = 514.5 nm	

Table 1.1: Key Dimensions and Physical Properties.

optimistic'' neutron inspiral strength for a detection rate of 3 events per year. Appendix A shows how detection rates for inspiraling neutron stars (the most concretely predictable expected source) depends on the dominant noise sources. The design philosophy is to trade off, where possible, the different noise sources to maximize the detection rate. This approach has resulted in a design with the expected maximum sensitivity, as shown in Figure 1.1, near 150 Hz.

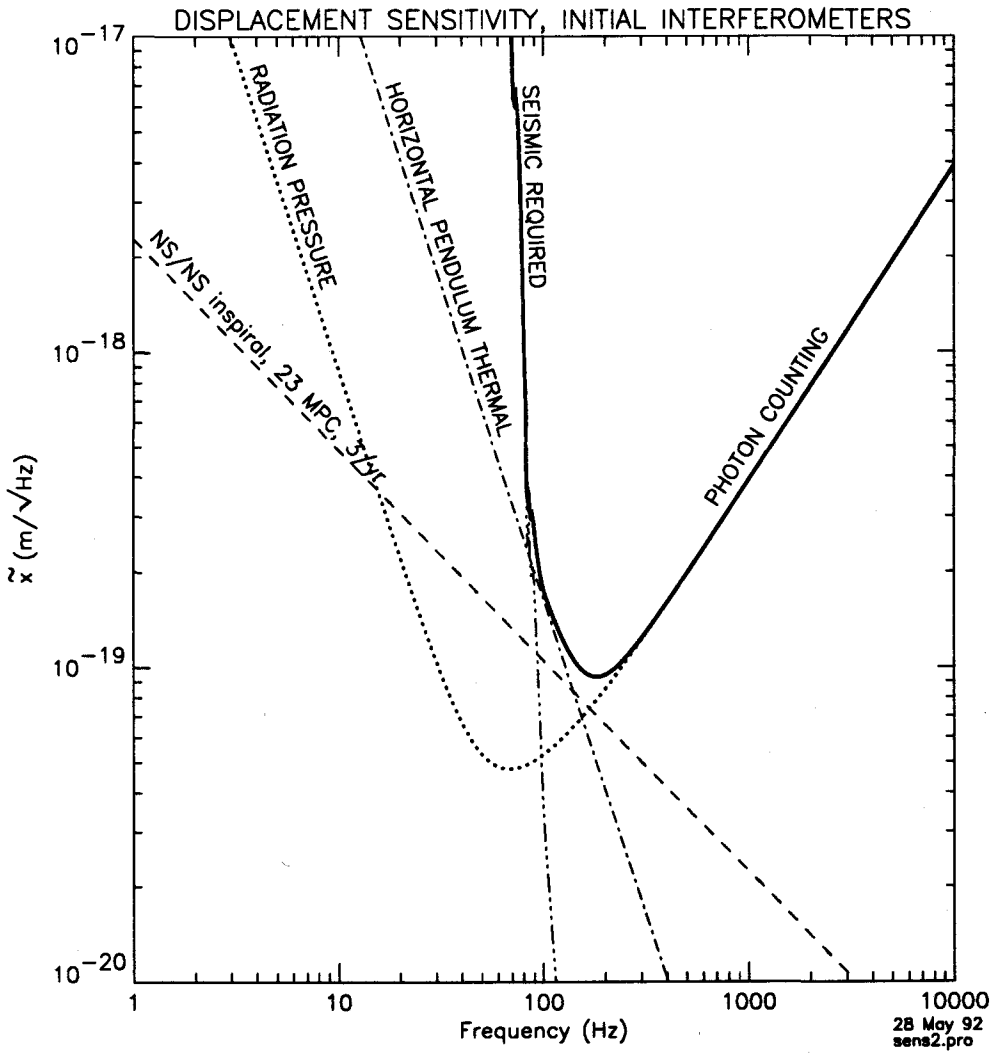

Figure 1.1: Expected displacement sensitivity of initial full-length (L = 4 km) LIGO interferometers (plotted with bold line), and contribution from the most significant noise sources. The *NS/NS inspiral* signal level was derived from Figure 10 of *Science* [3], by shifting that curve down by a factor of 11 to account for orientation and statistical corrections, and converting to displacement units by $\tilde{x} = h_c L/\sqrt{f}$. *RADIATION PRESSURE* and *PHOTON COUNTING* noise are the two types of shot noise discussed in Section 1.2.1 (Curve 2 of Figure 1.2 is plotted here); *SEISMIC REQUIRED* is the seismic noise described in Section 1.2.2; *HORIZONTAL THERMAL* noise is discussed in Section 1.2.3. Displacement noise levels are expected to be the same for half-length (L =2 km) interferometers, except photon counting (which is expected to be smaller) and radiation pressure (expected to be larger). The half-length and full-length interferometers will have the same power and storage times.

1.2.1 Shot Noise

Idealized Interferometer

The displacement sensitivity shot noise limit from photon counting at the main photodetector output of all initial LIGO interferometer configurations under consideration has the following frequency dependence:

$$\tilde{x}(f) = \tilde{x}_o\left(1 + [f/f_k]^2\right)^{1/2} \tag{1.1}$$

where f_k, the cavity knee frequency, is related to the arm cavity storage time by $\tau_e = 2L/c\mathcal{L}$ and to the mirror losses by $2\pi f_k = c\mathcal{L}/4L$; $\mathcal{L}$ is the total of transmission, absorption, and scattering losses for both mirrors making up an arm cavity of length L.

For a non-recycled interferometer,

$$\tilde{x}_o = \frac{\lambda}{2\pi}\mathcal{L}\frac{\sqrt{2}}{8\sqrt{\dot{N}}} \tag{1.2}$$

and the effective photon flux $\dot{N}$ is related to the efficiency-corrected power P incident on the beamsplitter by $P = \dot{N}hc/\lambda$. This result[1] applies to an idealized recombined system ([15], [2]) and also to an optimized modulated system where transmission is the dominant loss [13].

To extend this result to power recycling, $\dot{N}$ is replaced by $B_{\rm rec}\dot{N}$ (see Table 1.2 for definition of $B_{\rm rec}$).

Interferometers with Recycling and Modulation

The recycled interferometer shot noise has been calculated for a range of parameters in the externally modulated initial LIGO configuration under investigation at MIT [16]. The precise value of the shot noise depends on the arrangement of pick-offs and on the distribution of losses. As illustration, two optimized cases, identified as "Interferometer 1 with no contrast defect," and "Interferometer 3" (which includes an additional output cavity to pass "ω_3" sidebands), give shot noise levels corresponding to $1.22x_0$ and $0.83x_0$, respectively[2].

[1] Used to prepare the shot noise curves in the 89 Proposal [1], and in *Science* [3]. It is lower than the shot noise in the non-recombined configuration of the 40 m interferometer (in the low loss, low modulation limit) by $\sqrt{6}$.

[2] The "Interferometer 1" configuration with an assumed contrast defect of 1×10^{-3} has noise corresponding to $1.41x_0$ (not shown in figure 1.2).

A calculation of the unbalanced Michelson configuration under study at Caltech [10] gives a result very close to the "Interferometer 1, no contrast defect" result: $\sqrt{3/2}x_0 = 1.22x_0$.

Parameters and Comparison

The parameters relevant to shot noise and their values are listed in Table 1.2. Figure 1.2 shows the displacement sensitivity corresponding to different shot noise calculations.

Symbol	Description	Value	Notes
λ	Laser wavelength	514 nm	
L	Arm Length	4 km	
m	Cavity mirror mass	10.8 kg	Sets radiation pressure noise.
T_1	Input mirror power transmission	3%	T_1 assumed to be dominant loss. Noise insensitive to T_1 for $f > f_k$.
T_R	Transmission of recycling mirror	3.3%	
P_{circ}	Circulating power in arm cavities	3.9 kW	
I_{cav}	Intensity on cavity mirrors	540 W/cm^2 180 W/cm^2	@ input coupler @ output coupler
P_{BS}	Circulating power at beam splitter	60 W	
I_{BS}	Intensity on beam splitter	8.3 W/cm^2	
f_k	Knee frequency	90 Hz	$2\pi f_k = cT_1/4L$.
ηP	Power incident on recycling mirror	2 W	Corrected for inefficiencies. May be achieved, e.g., with 3 W out of input mode cleaner, 75% efficiency of remaining optics, and 90% photodetector quantum efficiency.
B_{rec}	Recycling factor	30	Defined as power buildup in arm cavities, compared to non-recycled cavities. Scattering and absorption losses alone allow larger B_{rec}; assumed limited by recombined beam contrast defect.

Table 1.2. Parameters that affect shot noise (high frequency) and radiation pressure noise (low frequency).

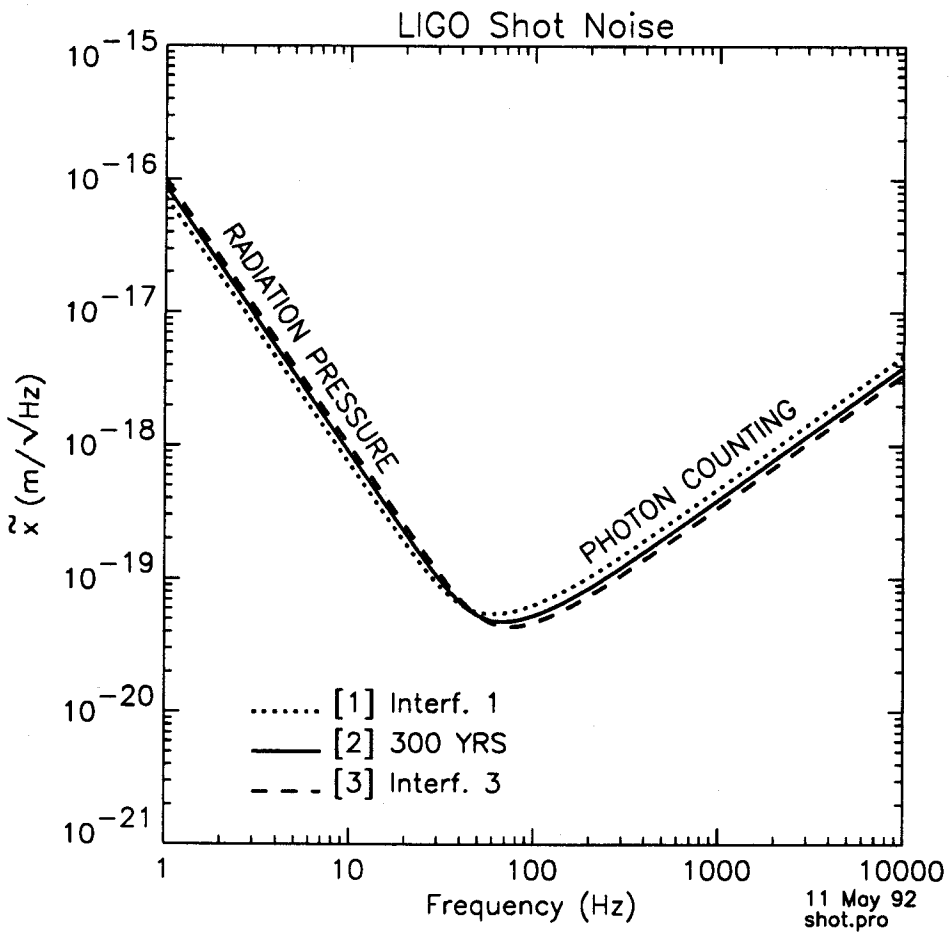

Figure 1.2. Shot noise calculation of photon counting and radiation pressure fluctuations for a system described by the parameters in Table 1.2. The radiation pressure lines intersect the photon-counting curves and the standard quantum limit (not shown; see [15]) at 41, 50, and 57 Hz, for curves 1, 2, and 3, respectively. Curves 1 and 3 are from [16], "Interferometer 1 with no contrast defect," and "Interferometer 3," respectively. Curve 2 corresponds to Equations 1.1 and 1.2. A preliminary calculation of the unbalanced Michelson variant [10] matches curve 1.

1.2.2 Seismic Noise

Linearly Coupled Seismic Noise

Ground motion excites an interferometer test mass after being filtered by an isolation stack and a wire suspension. To first order, the interferometer responds only to motions of the test masses along the beam line. Because of the curvature of the earth and misalignments, local vertical is not perpendicular to the beam line for all the test masses; consequently there is some contribution to interferometer noise from vertical motion of the test masses. Below approximately 90 Hz, the interferometer sensitivity is expected to be limited by direct linear coupling of seismic motion (assuming a 4 layer stack with viton as the elastomer). The strain noise due to seismic excitation is the product of 3 components:

1. Ambient ground motion
2. Stack isolation
3. Suspension isolation

Figure 1.3 shows the seismic noise requirement and goal for the initial LIGO interferometers. The "SEISMIC GOAL" curve shows the level of isolation that we believe can be achieved by the initial interferometer; it is significantly better than the "SEISMIC REQUIREMENT" level.

Components of Linearly Coupled Seismic Noise

The ground motion is determined by the specific sites that have been selected. Table 1.3 specifies a "standard spectrum" which is used as our basis for seismic noise estimates. It is a fit to measurements taken at locations throughout the United States. Ambient ground motion is fairly isotropic; consequently, the standard spectrum is the same in both the vertical and horizontal directions. Excitations due to tilts and rotations of the earth are assumed to be second order effects.

The ground noise is filtered through an isolation stack that functions as a passive low pass filter. The number of poles of the filter is twice the number of stack layers.

Since the test mass suspension wires are only 25 cm long, a connection between the top of the stack and the top of the test mass suspension is necessary for the test mass to reach the beam line (see Figure 1.4). This connector will be a rigid structure in the initial LIGO and will be termed the "vertical connecting

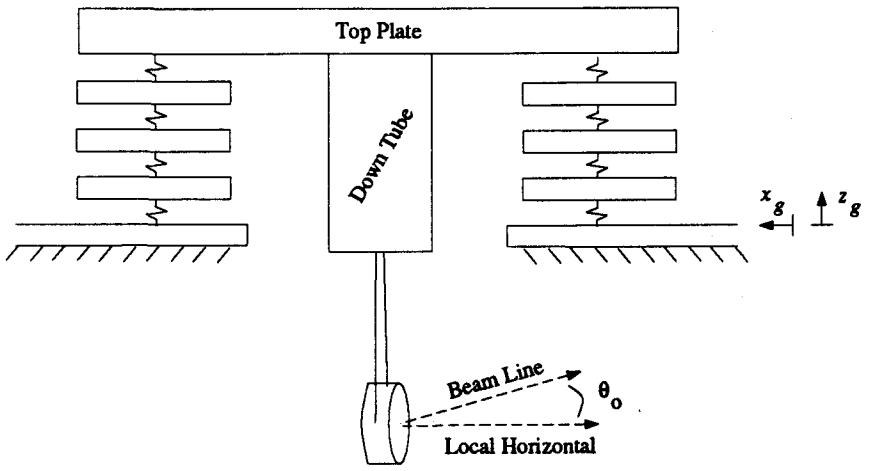

Figure 1.4: Possible Configuration of LIGO Test Mass Isolation System.

tube". The vertical connecting tube has a moment arm at least as long as the height of the stack; consequently, it will directly couple tilts from the top of the stack to horizontal motion of the test mass.

Additional filtering comes from a pendulum suspension connected to the base of the vertical connecting tube. The pendulum suspension acts as a seismic four pole low pass filter in both the horizontal and vertical directions.

The displacement noise spectrum $\tilde{x}$ due to seismic motion is a function of the stack and suspension parameters (see Table 1.4) and the horizontal and vertical ground motion x_g and z_g, respectively.

$$\tilde{x}(f) = \frac{2}{f^2}\left[\left[f_h^2 H_{xx} + f_h^2 R H_{\theta x} + \theta_o f_v^2 H_{zx}\right]^2 x_g^2 + \left[f_h^2 H_{zx} + \theta_o f_v^2 H_{zz}\right]^2 z_g^2\right]^{\frac{1}{2}} \tag{1.3}$$

Nonlinear Coupling

Larger low frequency (below approximately 15 Hz) motions of the test mass can also affect interferometer output in three ways:

1. Motions along the beam axis that perturb optical resonance.
2. Angular motions that change the pointing of the test mass.
3. Motions transverse to the beam line causing noise via irregularities in mirror scattering.

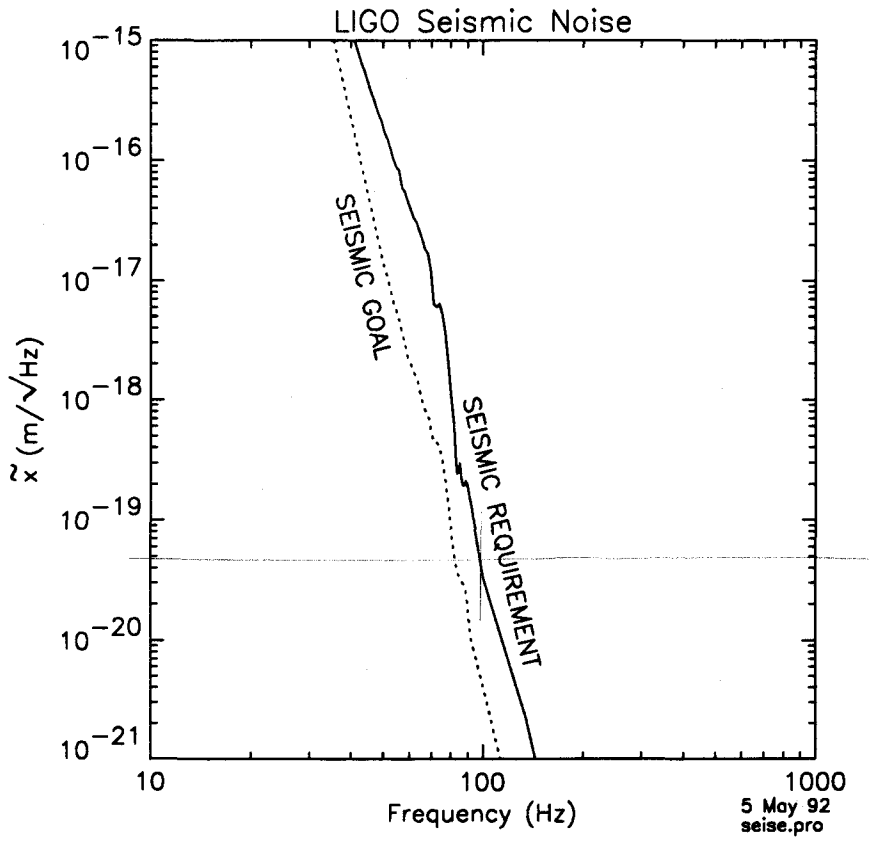

Figure 1.3: Requirement and Goal for Seismic Noise Contribution to Strain Spectrum.

FREQUENCY	AMPLITUDE
.1-1 Hz	$\frac{10^{-9}}{f^3}\frac{\text{m}}{\sqrt{\text{Hz}}}$
1-10 Hz	$10^{-9}\frac{\text{m}}{\sqrt{\text{Hz}}}$
10-10000 Hz	$\frac{10^{-7}}{f^2}\frac{\text{m}}{\sqrt{\text{Hz}}}$

Table 1.3: Adopted Standard for Ground Motion at LIGO Sites

Symbol	Description	Value
f_h	Pendulum horizontal resonance	1 hz
f_v	Pendulum vertical resonance	15 hz
θ_o	Angle of interferometer beam relative to local horizontal	.5 mrad
R	Height of vertical connecting tube	90 cm
H_{zz}, H_{xz}	Coupling coefficients from vertical ground motion to vertical and horizonal top plate motion, respectively.	see [14]
H_{zx}, H_{xx}	Coupling coefficients from horizontal ground motion to vertical and horizontal top plate motion, respectively.	see [14]
$H_{\theta x}$	Coupling coefficent from horizontal ground motion to the pitch angle of the top plate.	see [14]

Table 1.4: Stack and Suspension Parameters Used to Calculate Seismic Displacement Noise.

These higher order couplings, especially motions transverse to the beam line, are difficult to quantify.

The requirement on low frequency motion along the beam axis is stated in terms of rms motion of the test mass and is as follows: the total differential motion of a test mass must be less than 6×10^{-11}m. This level of motion keeps the effective storage time of each arm cavity matched to 1% [12]. The requirement on the total angular motion of a test mass is dictated by the contrast. In order to maintain a contrast in the interferometer of $C > \left(1 - 1 \times 10^{-3}\right)$, the rms alignment of the LIGO cavities must be held to within 2×10^{-7}rad (see [12] for a more detailed discussion). Servo loops are required to reach these low levels of RMS motion since the net horizontal single mirror motion is estimated to be 3.5×10^{-7} m RMS and the net angular single mirror motion around the vertical axis is estimated to be 3.5×10^{-7} rad RMS [12]. There is as yet no specification for the maximum allowed test mass motions transverse or vertical to the beam line; consequently, it has not been determined whether transverse or vertical damping of the test mass is necessary.

The requirement on motion of auxiliary optics is not as stringent, but has not yet been specified.

1.2.3 Thermal Noise

Each mode of a mechanical system has $\frac{1}{2}k_BT$ of energy (k_B the Boltzmann constant, T the absolute temperature). Equating this energy with the average kinetic energy of an oscillator $mv^2/2 = m\omega_0^2x^2/2$ of the mode of (effective) mass m and resonant frequency ω_0 allows us to calculate the mean-square displacement $x_{\text{thermal RMS}} = \sqrt{k_bT/m\omega_0^2}$. This motion will be distributed in frequency according to the losses in the oscillator.

If the losses are due to viscous damping (force F proportional to the velocity, $F = -\alpha v$; e.g., a dashpot), then the displacement noise spectrum is

$$\tilde{x}(f) = \left[\frac{4k_BT\alpha}{\left(k - m(2\pi f)^2\right)^2 + \alpha^2(2\pi f)^2}\right]^{\frac{1}{2}} \frac{\text{m}}{\sqrt{\text{hz}}} \tag{1.4}$$

The restoring force (gravity for the horizontal mode of the pendulum, or the material stiffness for a mirror internal mode) is represented by $F = -kx$, where the unsubscripted k is the usual Hooke's spring constant ($\omega_0 = \sqrt{k/m}$). The quality factor Q is related to the damping coefficient by $Q = m\omega_0/\alpha$.

Although experimental data confirmation is needed, we believe that the most likely loss mechanism for most of the critical LIGO systems is an internal damping which gives a force proportional to the displacement $F = -\phi(f)x$. This may be parameterized by a complex force constant: $F = -k(1 + i\phi(f))x$, giving a spectrum of displacement:

$$\tilde{x}(f) = \left[\frac{4k_BTk\phi(f)}{2\pi f\left(\left[k - m(2\pi f)^2\right]^2 + k^2\phi(f)^2\right)}\right]^{\frac{1}{2}} \frac{\text{m}}{\sqrt{\text{hz}}} \tag{1.5}$$

Equations 1.4 and 1.5 are plotted in Figure 1.5 with ϕ equal to a constant (the most likely case). The two curves differ because of the extra f in the denominator of the internally damped curve, giving a slope of $f^{-1/2}$ below the resonance and a slope of $f^{-5/2}$ above the resonance. We specify ϕ in terms of an equivalent internal damping on resonance $Q_{id} = 1/\phi$ to compare with viscous damping. See [11], page 243 for more detail and discussion.

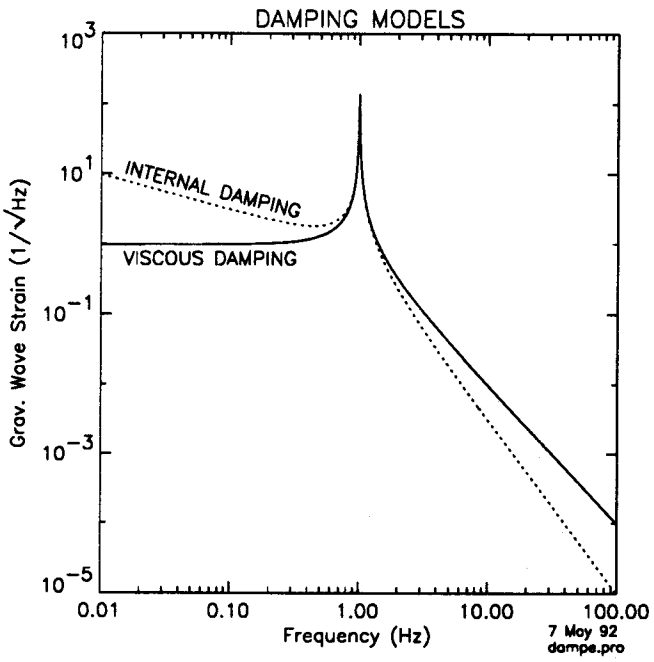

Figure 1.5: Resonance Curves for Viscously Damped System and Internally Damped System.

Estimates of the thermal noise based on material and design parameters are adopted as the requirements. To deal with the lack of experimental data, we choose the more conservative model for loss when determining the performance requirement.

Thermal Noise in Pendulum Suspensions

In the pendulum suspension, we are concerned with the thermal noise above resonance; the pendulum has a horizontal mode at roughly 1 Hz. The number, shape, and kind of suspension fibers and the terminating impedance of the suspension wires at the pendulum support point determine the thermal noise level .

For the calculations here, we assume a single tungsten wire loop which forms the suspension for a cylindrical test mass. The suspension wires are assumed to be stressed at about half their breaking strength. The parameters used for the model of the suspension are summarized in Table 1.5. This results in a horizontal pendulum frequency of $f_h = 1$ Hz, and a vertical pendulum frequency of $f_v = 15$ Hz.

PROPERTY DESCRIPTION	VALUE
Tungsten Wire Density	$15 \times 10^3 \frac{kg}{m^3}$
Wire Radius	1×10^{-4}m
Pendulum Length	.25m
Young's Modulus	$3.5 \times 10^{11} \frac{N}{m^2}$
Mirror Mass	10.8kg
Temperature	300°K

Table 1.5: Parameters Used In Suspension Model.

We choose a conservative model for the damping mechanism, and an optimistic Q for the interferometer requirement: viscous damping as described by Equation 1.4 and a $Q = 10^7$. Measurements of the internal loss of suspension wire materials are not in contradiction with this Q value, although there is no direct measurement to support it. The resulting displacement noise is shown in Figure 1.6 and falls as $1/f^2$ above 1 hertz.

The vertical oscillation of the pendulum also exhibits thermal noise. As above, the loss mechanism is not well understood, and so the more conservative viscous damping is assumed. The Q_v is expected to be lower than for the horizontal pendulum because the oscillator energy is stored in the wire, not in the earth's gravitational field. The pendulum vertical Q is taken to be $Q_v = 10^4$. For the motion to appear on the optic axis, a cross coupling from vertical motion of the pendulum wires to horizontal motion of the mirror is needed. It is sure to be at least .5 mrads (due to the curvature of the earth over 4 km), but may be greater due to lack of levelness of the site or imperfections in the suspension; we use 5×10^{-4}. The displacement noise is shown in Figure 1.6 and falls as $1/f^2$ above 15 hertz.

The transverse suspension wire mode ('violin string' resonance) thermal noise will not limit the noise floor of the interferometer, but will present a series of narrow spectral peaks spaced at (approximate) multiples of the fundamental frequency which with likely suspension properties will be about 650 Hz. We take a simple model where the excitation of the wire modes is calculated using either Equation 1.4 or 1.5, then the impedance mismatch going from the wire to the mass is used to calculate the resulting motion of the test mass. We use here a separately determined Q for the transverse modes. We ignore any contribution from the longitudinal modes of the suspension.

The $Q_{\text{string}_{id}}$ for the fundamental string mode on resonance is taken to be 3×10^5. An internal damping model is assumed. The expected noise is indicated in Figure 1.6 as "WIRE". The peak value of the fundamental string mode at 650 Hz is about $10^{-20} \frac{\text{m}}{\sqrt{\text{Hz}}}$.

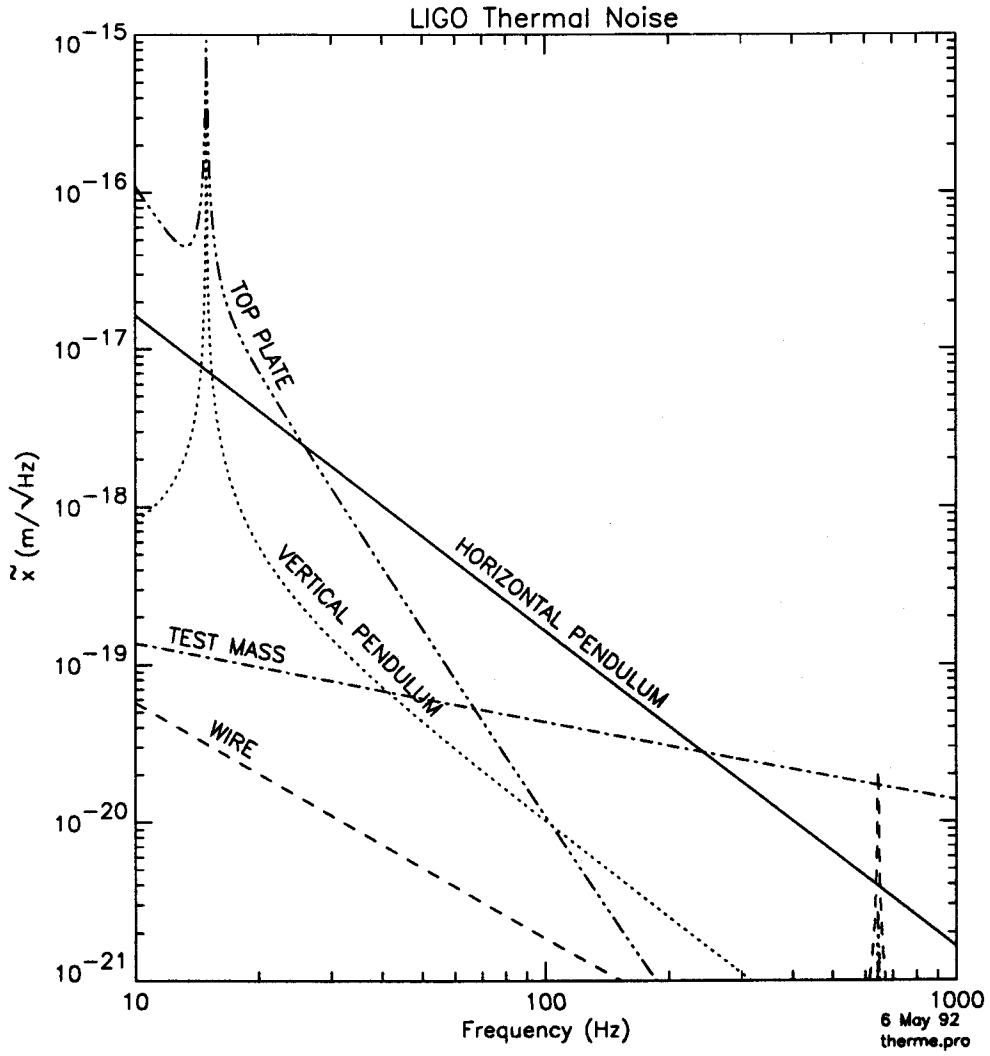

Figure 1.6: Thermal Noise Contribution to Strain Spectrum.

Thermal Noise in the Seismic Isolation Stack

The seismic isolation stack is a resonant system that exhibits thermal noise. We analyze only the oscillatory system consisting of the top plate mass and the springs/dampers upon which it sits, and disregard the remainder of the stack due to its second order contribution.

The horizontal oscillation (direct excitation of the suspension point) and the horizontal rotational oscillation (coupled through the vertical connecting tube) between the stack top plate and the pendulum suspension point) are considered. The parameters for the model are taken from the LIGO prototype stack, Jan '92. In this design, a deliberate low Q is chosen for the resonances (to reduce the level of motion due to seismic excitation on the resonance). The loss as a function of frequency for the Viton elastomer used as the spring and damper in the stack has been measured to be roughly constant with frequency. To be on the conservative side, though, a viscous damper model with a $Q_{\text{stack}} = 5.0$ is used. The other parameters are m=100 kg, $\omega_{o_h} = 2\pi \times 2$ Hz, $\omega_{o_v} = 2\pi \times 6$ Hz, coupling vertical to horizontal (vertical connecting tube length)/(stack top plate diameter)= 1.0. Note that the level at a given frequency grows as $\omega_o^{1/2}$. This excitation is filtered by the suspension pendulum, which is assumed to have a transfer function of $\left(\omega_{o_{\text{pend}}}/\omega\right)^2$, $\omega_{o_{\text{pend}}} = 2\pi \times 1$ Hz; this leads to the displacement noise shown in Figure 1.6. The curve is labelled "TOP PLATE" and falls as f^{-4}.

Thermal Noise in Mirror Substrates

The mirror substrate resonant frequencies lie above the gravity wave band, so we are interested in the thermal noise below the resonant frequency. The first few piston and annular resonant modes of the test mass contribute significantly, as does the + mode (two radial nodal lines at 90^o) which is derated based on the symmetry of the beam on the + mode.

As in the case of the pendulum, the correct model for the thermal noise has not been determined (although there is an experiment underway [9]). The more conservative estimate comes from an assumption of internal damping (ϕ=constant). A large high-quality substrate has shown measured Qs of 2×10^5 to 4.5×10^5 for several modes [4]. Further experiments with attachments and means of suspension are needed (and are underway in Orsay and Caltech).

The internal damping is taken to be that due to a Q on resonance of $Q_{\text{mirror}_{\text{id}}} = 10^6$. The mode frequencies used are 9.5×10^4 Hz (+ mode, with

a derating factor for the + mode of 10^{-1}), 1.4×10^4 Hz for a flexure mode with a circular nodal line (the dominant contribution), and a series of longitudinal modes starting at 2.8×10^4 Hz. Figure 1.6 shows an estimate of the thermally induced displacement noise and is labeled "Test Mass". It was calculated using the quadratic sum of the substrate modes. The curve has a slope of $1/\sqrt{f}$ at frequencies below the first substrate mode.

1.2.4 Other Noise Sources

Residual Gas Noise

1.3 Design Overview

The proposed basic design is a combination of the design outlined in the 1989 LIGO proposal [1] and subsequent designs and demonstrations. As shown in Figure 1.7, the overall Gravitational Wave Interferometer can be divided up into four major systems: an Input Optics System, an Interferometer System, a Data Acquisition and Interferometer Operations (DAIO System), and an Environmental Monitoring System.

The Input Optics System generates and conditions the laser light for the interferometer system. The prestabilized laser is a modified single Argon ion laser capable of an output power of 5 W (single mode). This laser is both frequency and amplitude stabilized by active servo loops. The mode cleaner subsystem will use a combination of one or more resonant Fabry–Perot cavities in transmission to stabilize further the frequency, amplitude, position and direction of the light. This will be followed by a set of injection optics which will mode match, point and otherwise condition the beam prior to passing it to the interferometer system.

The Interferometer System is the central part of the Gravitational Wave Interferometer. The optical interferometer senses the motion of test masses at the ends of the interferometer. The interferometer will operate in a Michelson configuration, with Fabry–Perot cavities in each arm to increase the sensitivity. The Fabry–Perot cavity in each arm of the interferometer will have a storage time of roughly 2 ms. Broadband recycling in the Michelson interferometer will be used to increase the circulating light power by a factor of 30. The differential phase shift induced by gravitational strain may be detected by interfering the light from the Michelson beamsplitter's antisymmetric output port with a phase modulated reference beam, derived from the illuminating light, in an external Mach–Zehnder interferometer arrangement, or by intentionally creating a small imbalance in the Michelson interferometer which will cause a small modulation of the light at the dark port. Pendulum suspensions will be used for the optical components, with active damping and steering from local sensors and drivers. A passive isolation stack employing unencapsulated elastomer springs will be used as the first stage of seismic isolation. An automated optical alignment system will be intrinsic to the design of the interferometer and will provide signals to the suspension and control system to control the alignment of the interferometer.

The DAIO System will monitor and control adjustable parameters of the system, as well as record all data from the Interferometer, Input Optics, and Environmental Monitoring System necessary to analyze the output for gravitational wave signals. The breakdown of the DCS into subsystems is not yet determined.

The Environmental Monitoring System consists of the instrumentation that monitors environmental factors that influence the interferometer's performance. Such factors include background magnetic field, seismic background at the vertex and end stations, cosmic ray background, temperature, etc. The Monitoring system interfaces with the DAIO system where the data is used for vetoing possible astronomical events that correlate with significant environmental events. The breakdown of the Environmental Monitoring System has not yet been determined.

1.3.1 Handbook Organization

The structure of the handbook follows closely the functional blocks pictured in Figure 1.7. Each of the major subsystems is described in its own chapter. Each subsystem is then broken into its own set of constituent blocks. The subsystem blocks were chosen to maximize the testability of each of the blocks. There is overlap in the design of many of the functional blocks since some of the components that appear in one block also appear in other blocks. For example, there is a seismic isolation subsystem (which is a part of the Interferometer System) and there is seismic isolation as a part of the mode cleaner. Rather than attempting to eliminate all such cases, we have adopted the working assumption that any overlap should be handled by cross-reference. In this example, the description of the mode cleaner seismic isolation would reference one of the standard designs of the seismic isolation subsystem, with any special requirements or modifications noted. Information that supplements the design effort can be included in the Appendix of the handbook or referenced to other documentation (such as the LIGO Working Papers).

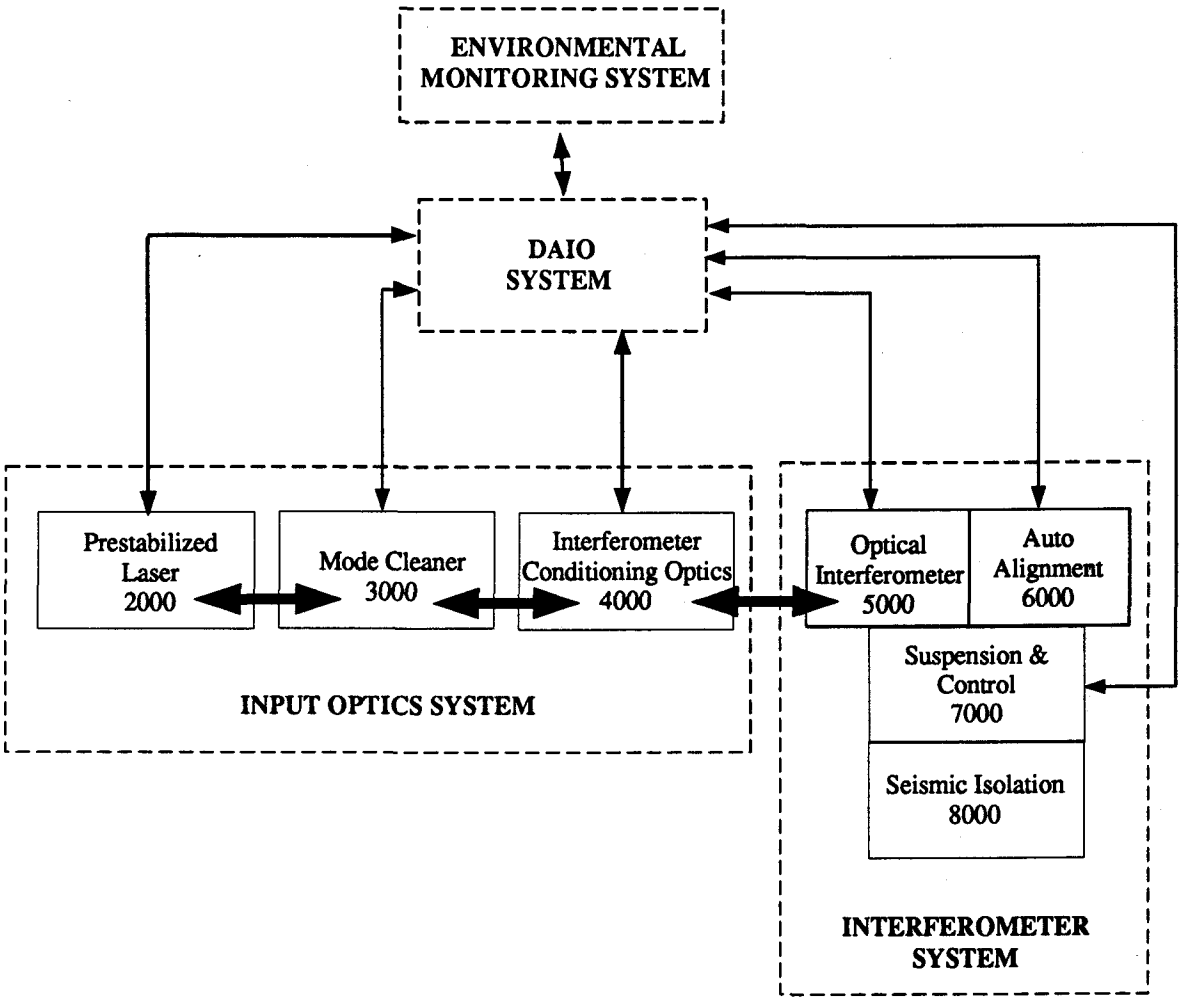

Figure 1.7: Functional Blocks of Gravity Wave Interferometer.

Chapter 2
ICD 2000 Prestabilized Laser

The function of a prestabilized laser subsystem is to provide an interferometer with light at a wavelength of 514.5 nm. It should operate at a sufficient power level, and provide adequate beam conditioning, so that the required interferometer sensitivity can be achieved.

There will be one prestabilized laser subsystem per interferometer; consequently, two subsystems at Site 1 and one subsystem at Site 2.

2.1 Functional Requirements

1. The prestabilized laser will deliver 3.5 W output power. This will ensure a minimum of 2 W at the recycling mirror.
2. The light delivered to the input optical chain will have its frequency stabilized down to 10^{-2} Hz/Hz$^{1/2}$, above 1 kHz, and down to a limit that is slowly increasing towards lower frequencies. This is shown explicitly in Figure 2.1. Frequency fluctuations at this level can be suppressed by frequency stabilization servo systems downstream, to a level compatible with LIGO sensitivity requirements.
3. The frequency of the prestabilized laser is meant to track the length of the mode cleaner. This will be achieved by feeding the error signal, derived at the mode cleaner, back to the laser, which will function as a voltage controlled oscillator (VCO). The two inputs for the tracking signal are called "slow VCO", and "fast VCO".
4. Relative optical power fluctuations will be kept down to 3×10^{-7} /Hz$^{1/2}$, above 1 kHz, and down to a limit that is slowly increasing towards lower frequencies (see Figure 2.2). At this point, this requirement is somewhat artificial, and is meant to improve upon the raw intensity noise of the laser currently used with the 40 m prototype.